Physica C 510 (2015) 21–26

Contents lists available at ScienceDirect

Physica C

journal homepage: www.elsevier.com/locate/physc

Smooth surfaces in very thin $GdBa_2Cu_3O_{7-\delta}$ films for application in superconducting tunnel junctions

H. Navarro [a,b,*], M. Sirena [a,b], Jeehoon Kim [c,d], N. Haberkorn [a,b]

[a] Instituto Balseiro, Universidad Nacional de Cuyo & CNEA, 8400 Bariloche, Argentina
[b] Centro Atómico Bariloche, Comisión Nacional de Energía Atómica. Av. Bustillo 9500, 8400 San Carlos de Bariloche, Argentina
[c] Department of Physics, Pohang University of Science and Technology, Pohang, Republic of Korea
[d] CALDES, Institute for Basic Science, Pohang, Republic of Korea

ARTICLE INFO

Article history:
Received 31 October 2014
Received in revised form 10 December 2014
Accepted 28 December 2014
Available online 6 January 2015

Keywords:
Thin films
Superconductivity
Morphology

ABSTRACT

This paper provides a systematic analysis of the morphology and the superconducting critical temperature obtained in very thin $GdBa_2Cu_3O_{7-\delta}$ films grown on (001) $SrTiO_3$ substrates by DC sputtering. We find that the use of a very thin $SrTiO_3$ buffer layer (≈2 nm) modify the nucleation of $GdBa_2Cu_3O_{7-\delta}$ on the surface of the substrate reducing the formation of 3 dimensional clusters. Our results demonstrate that 16 nm thick $GdBa_2Cu_3O_{7-\delta}$ films with an average root-mean-square (RMS) smaller than 1 nm and large surface areas (up 10 μm^2) free of 3 dimensional topological defects can be obtained. In films thinner than 24 nm the onset (zero resistance) of superconducting transition of the films is reduced, being close to liquid nitrogen. This fact can be associated with stress reducing the orthorhombicity and slightly drop in oxygen stoichiometry.

1. Introduction

The high-T_c superconductors (HTS) such as $RBa_2Cu_3O_{7-\delta}$ (RBCO; *R*: Y, G, Eu) have a large potential in technological applications. Potential superconducting applications (such as superconductor–insulator–superconductor (SIS) structures, Josephson junctions (JJ), and superconducting quantum interference devices (SQUID)) require epitaxial films and abrupt interfaces [1,2]. The advantages of HTS in these devices are based on a much higher operating temperature ($T_c \approx$ 90 K), and higher energy gap [3–5] than low T_c superconductors. This gap allows the development of electronic systems operating in the THz range [6,7]. Although advances have been made in the development Josephson junctions by ion irradiation in YBCO films [6], the main limitation to the development of SIS devices using HTS is given by the morphological features of the bottom superconducting electrode which limits the quality of the insulator barrier.

HTS thin films usually present a complex growth mechanism, which affects both morphological and superconducting properties [8,9]. For SIS development and in order obtain an homogenous insulator layer [10], smooth surfaces (low roughness) and large flawless areas are necessary [11]. The initial states in YBCO thin films depend on the substrate and the deposition parameters. $SrTiO_3$ (001) single crystals are usually used as substrate for HTS thin films due to their chemical compatibility and nearly matching lattices. The resulting properties in very thin HTS films on $SrTiO_3$ (001) are affected by the surface termination. The presences of different stacking interface sequences induce the formation of anti-phase boundaries by coalescence of islands [8], due to different terminating layer in the substrate (e. g. $SrTiO_3$ surface can be TiO_2 or SrO). YBCO films grow on $SrTiO_3$ layer-by-layer mode followed by islands growth [12,13]. The thickness at which the growth of thin films switches from layer-by-layer to island growth was estimated to vary from 10 nm to 19 nm for YBCO on $SrTiO_3$. For thicknesses beyond 38 nm, spiral growth features emerge in YBCO [12]. The 3D screw-dislocation (or island nucleation growth mode) plays an important role in applications that require high critical current densities [9]. Very thin HTS films present a suppressed superconducting critical temperature (T_c) due to an increment the in-plane ordering, which strongly indicates that the presence of defects favors the oxygen in-diffusion and relaxes the strain at the interface with the substrate [14]. Due to substrate-induced strain, YBCO films thinner than 11.5 nm are tetragonal. Above this critical thickness they gradually evolve towards the bulk orthorhombicity of fully oxygenated YBCO at thickness ≈24 nm [14]. The effect of the stress affecting the orthorhombicity

* Corresponding author at: Centro Atómico Bariloche, Comisión Nacional de Energía Atómica. Av. Bustillo 9500, 8400 San Carlos de Bariloche, Argentina. Tel.: +54 0294 444 5171; fax: +54 0294 444 5299.
E-mail address: henrynavarro@cab.cnea.gov.ar (H. Navarro).

http://dx.doi.org/10.1016/j.physc.2014.12.010
0921-4534/

of $GdB_2Cu_3O_{7-\delta}$ thin films is also manifested in a reduction of the carrier density [15].

In this paper, a study of the initial stages in the growth of GdBCO films by atomic force microscopy force (AFM) is being reported. It was found that by using a very thin $SrTiO_3$ (STO) buffer layer (2 nm) the GBCO nucleation was modified, and the topological defect density is considerably reduced [16]. This fact is attributed to the reconstruction of the $SrTiO_3$ surface [17] and to the reduction of anti-phase boundaries by coalescence of islands or terraces [7]. Results show that GdBCO films with thicknesses below 20 nm present a 2D growth-like mechanism. In films with thicknesses between 20 and 30 nm emerge a high density of 3D clusters with a large increment in the surface roughness. The use of a very thin $SrTiO_3$ (STO) buffer layer (2 nm) modifies the GdBCO nucleation, which considerably reduces the formation of 3D clusters with concomitant reduction of the surface defects. Films with thickness of 16 nm and RMS < 1 nm (<1 GBCO unit cell) and large areas free of topological defects can be obtained. This analysis contributes to the optimization of the bottom superconducting electrode for the development of SIS based on HTS.

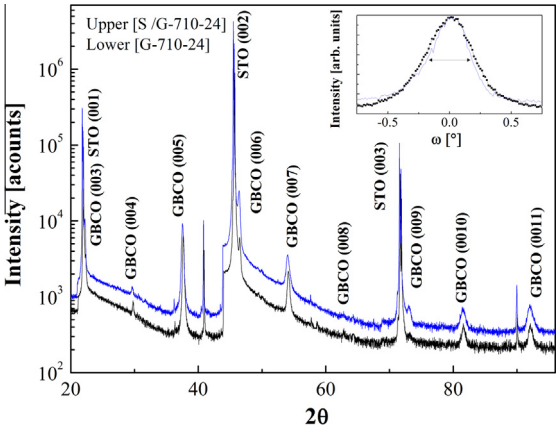

Fig. 1. X-ray diffractogram (logarithmic intensity scale) of the [G-710-24] and the [S/G-710-24] films at room temperature. The inset shows the rocking curves for the (005) reflection.

2. Experimental

Films of $GdBa_2Cu_3O_{7-\delta}$ (GBCO) on $SrTiO_3$ (001) (STO) substrates by DC magnetron sputtering were deposited at 400 mtorr total pressure (90:10 Argon:oxygen) and a power of 25 W. Prior to the deposition, the STO substrate was heated in air at 900 °C for 20 min. During the growth, the not aligned chopped power oscillatory (NACHOS) configurations were used [18]. The GBCO growth rate is 1.6 nm/min. Films with different temperatures of substrate were deposited at 710 °C, 730 °C, 750 °C and 760 °C. By the end of the deposition, the substrate was cooled down to 500 °C and the chamber was flooded with pure oxygen to a pressure of 100 torr. After that, the films were cooled down to room temperature at a rate of 1 °C/min. As it was mentioned above, films with and without STO buffer layer of 2 nm were grown. The deposition temperature for the buffer layer was the same than the one used for the GBCO deposition. The STO buffers were grown by radio frequency sputtering using a power of 25 W, which results in a deposition rate of 1 nm/min. GBCO films with final thicknesses (t) of 5 nm, 16 nm, 24 nm, 32 nm and 48 nm were grown with and without a buffer layer at 710 °C. On the other hand, films with a buffer layer (STO $\approx$ 2 nm) and t = 16 nm were grown at deposition temperatures of 710 °C, 730 °C, 750 °C and 760 °C. Wherever used, the notation [G–T_d–t] indicates a GBCO film (without buffer) with deposition temperature T_d [°C] and thickness t [nm]. The notation [S/G–T_d–t] indicates GBCO films with a STO (t = 2 nm) buffer layer.

AFM measurements were performed in a Dimension 3100 ©Brucker microscope. A detailed morphological characterization of the films was made by analyzing the topographic information at different scale lengths (1 μm and 10 μm). The AFM images presented in this work were performed in tapping mode. In order to avoid any chemical segregation (by humidity) or contamination of the surface, all the images were obtained after the growth without further manipulation. The structure of the films was analyzed by XRD using a Panalytical Empyrean equipment. The superconducting transition temperature was obtained by performing resistance versus temperature measurements with the conventional four-probe geometry.

3. Results and discussion

Fig. 1 shows X-ray diffraction pattern of the [G-710-24] and the [S/G-710-24] films. Similar X-ray diffraction pattern were obtained for the rest of the films. X-ray diffraction confirmed the c-axis orientation of the films. The rocking curves for the (005) GBCO line exhibit a full width at half maximum values of 0.45(5)° and 0.35(5)°, for films with and without buffer, respectively (see inset Fig. 1).

Fig. 2 shows a systematic analysis of GBCO films grown at 710 °C with thicknesses between 5 and 32 nm by AFM (10×10 μm^2 images). The results include films with and without a buffer layer. The films [G-710-5] and [S/G-710-5] present smooth surfaces (see Figs. 2a and 1b). The AFM profiles (not shown) show that the surface of the films present terraces with size of 200(20) nm and 300(30) nm, respectively. The presence of large terraces can be associated with a 2D growth-like behavior, as was previously reported for very thin YBCO films [8]. The small size of the terraces in [S/G-710-5] is attributed to a reduction of the anti-phase boundaries at the interfaces, which reduces the defect density by the coalescence between different nucleation places. As will be discussed below, these films are not superconducting (no percolation has been observed). Fig. 2c and d presents the AFM images in the [G-710-16] and [S/G-710-16] films. The image of [G-710-16] reveals3D topological defects formation (height > 20 nm), which considerably increase the surface roughness. The [S/G-710-16] film presents a remarkably low density 3D cluster in areas above 10 μm^2. The differences between the morphology of pure and buffered films are significant in films with a thickness of 24 nm (see Fig. 2e and f). The STO buffer layer reduces the apparition of 3D structures. Despite the differences clearly observed in the defect density, both samples show emergent 3D clusters with a concomitant increment of the surface roughness. The 2D to 3D change in the growth mechanism between 16 and 24 nm determines the shape and density of the topological 3D defects in thicker films (see Fig. 2e and f) [14]. A change from 2D-like to 3D growth mechanism has been observed, which is clearly manifested in thicknesses above 20 nm. However, the inclusion of a STO buffer layer improves the film surface quality reducing significantly the presence of 3D topological defects. Fig. 3a shows the average root-mean-square (RMS) roughness versus t obtained from Fig. 2. Films without buffer always present higher RMS (t) values. The first stages of the GBCO nucleation affect the thickness dependence of the morphology due to the emergence of small 3D structures. The smaller RMS value [S/G-710-5] can be associated with a small density of anti-phase boundaries due to the nucleation on the reconstructed surface of the STO [16]. On the other hand, for films thinner than 20 nm, the modification of the initial nucleation reduces significantly the density of 3D structures. The histograms of peak height profile obtained from the AFM images are shown

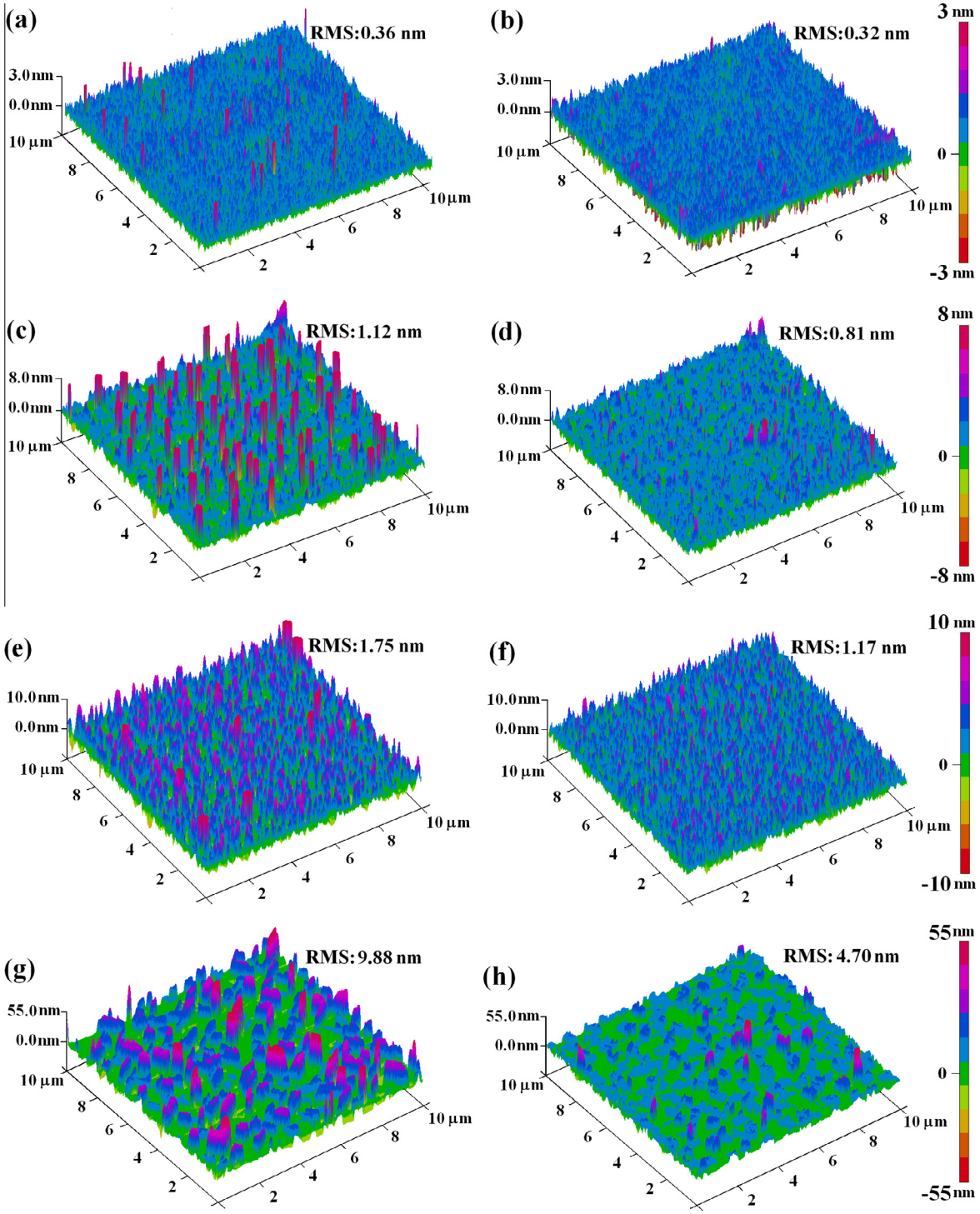

Fig. 2. 10 × 10 μm² topographical images of GBCO thin films deposited at 710 °C with and without a STO buffer layer: (a) [G-710-5]; (b) [S/G-710-5]; (c) [G-710-16]; (d) [S/G-710-16]; (e) [G-710-24] (f) [S/G-710-24]; (g) [G-710-32]; (h) [S/G-710-32]. The *Z*-scale ranges for each thickness are indicated in the figure.

in Figs. 3b–d. The histograms corresponding to [G-710-5] and [S/G-710-5] present similar features and a narrow distribution (no shown). The distribution in [G-710-5] shows a small asymmetry to negative *Z* values (holes), which can be associated with a high density of grain boundaries (small grains). At high thicknesses the histograms are asymmetric. The evolution of the film roughness with film thickness is manifested in wide bells, whereas the apparition of 3D defects produces asymmetric curves (to large Z values) and a bimodal distribution (see arrows in Fig. 3c and d) as consequence of the formation of 3D structures. The large density and big size of 3D topological defects in samples without buffer layers can be also clearly observed. For example, its average height in [G-710-32] is twice than in [S/G-710-32]. Features associated with the initial stages of the 3D clusters (asymmetric histogram) are evident in [G-710-16]. This asymmetry appears for $Z \approx 2.4$ (see Fig. 3b), which corresponds to steps of 2 u.c. of GBCO. On the other hand, the STO buffered GBCO films with $t \approx 16$ nm are to the limit for the formation of 3D structures.

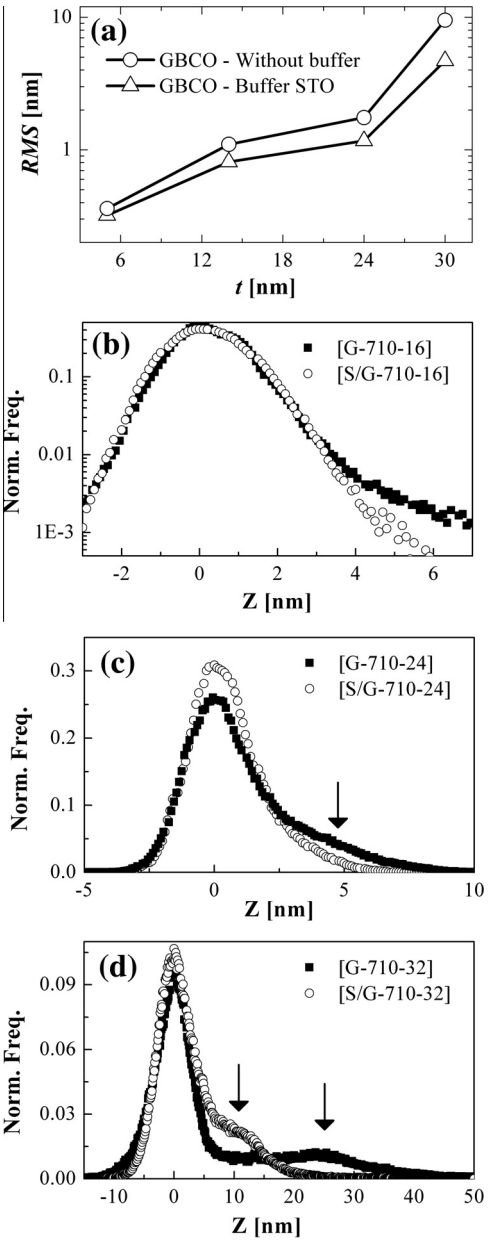

Fig. 3. (a) Thickness dependence of the RMS roughness of pure and STO buffered GBCO thin films. (b)–(d) Histograms of peak height profile for the different films based on the AFM images shown in Fig. 2. The frequency was normalized by the area under the curves. Arrows indicate a bimodal distribution by 2D and 3D growth.

Subsequently, in order to analyze the influence of the deposition temperature on the resulting morphological properties of the films, [S/G-730-16], [S/G-750-16] and [S/G-760-16] were grown. Fig. 4 shows the corresponding AFM images. The density of 3D topological defects is large when the deposition temperature is gradually increased from 710 °C to 730 °C, 750 °C and 760 °C (see Fig. 5). The tail to high Z values (asymmetry in the bell curves) evidences the 3D structures. The nucleation of 3D defects is even more drastic in films without buffer layer (not shown). The evolution of the film roughness as function of the deposition temperature indicates that surface mobility also contributes to the morphology of the films. Fig. 6 shows a comparison between the islands of the films [S/G-710-16] and the [S/G-730-16]. Steps of ≈2.5 nm are observed between islands (terraces), which is consistent with an integer number of GBCO unit cells (≈1.2 nm)

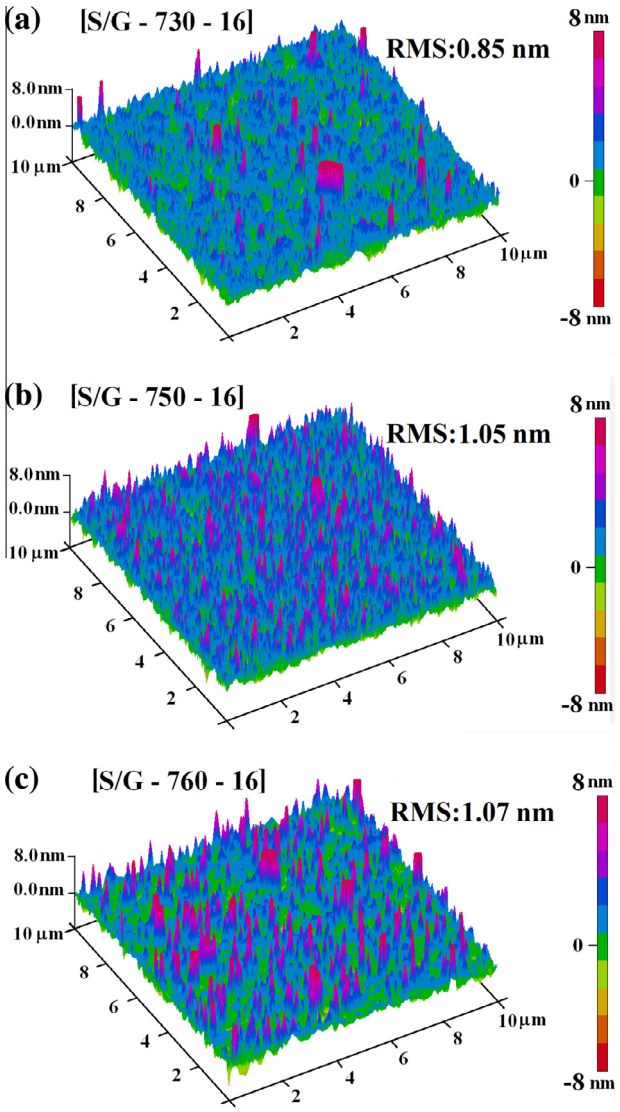

Fig. 4. 10 × 10 µm^2 topographical AFM images of: (a) [S/G-730-16]; b) [S/G-750-16]; and (c) [S/G-760-16].

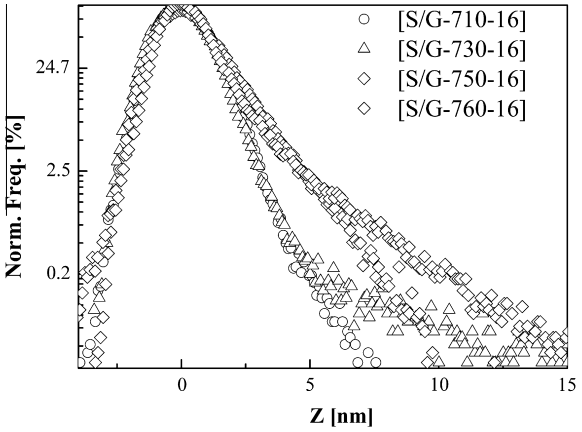

Fig. 5. Histograms of peak height profile for GBCO films deposited at different temperatures. The histograms are based on the AFM images shown in Fig. 2 (only [S/G-710-16]) and in Fig 4. The frequency was normalized by the area under the curves.

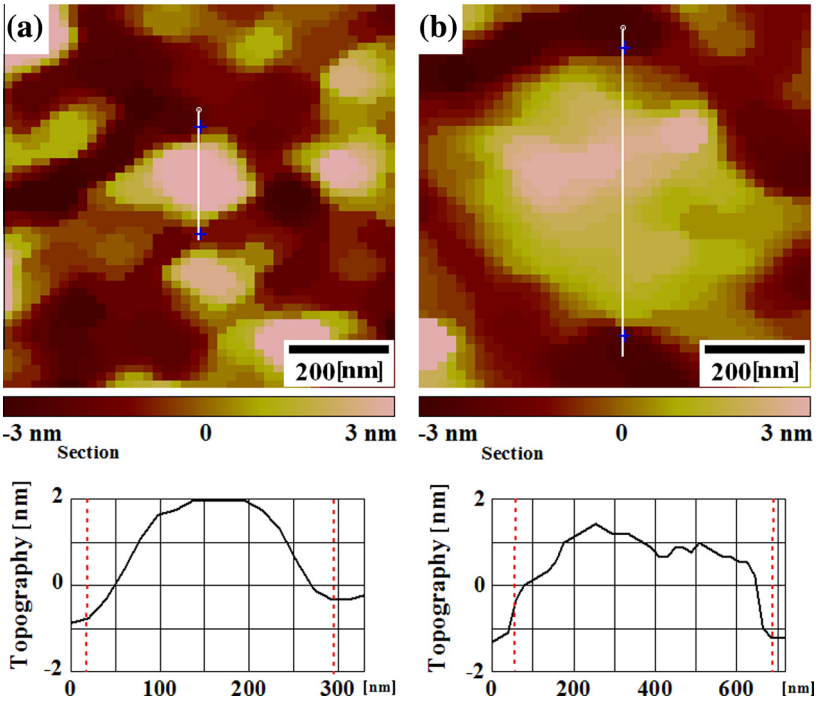

Fig. 6. (a) and (b) Topographic analysis of a surface defect in [S/G-710-16] (left) and [S/G-730-16], and their corresponding AFM profiles.

[9]. The terrace size for the films deposited at 730 °C (≈650(50) nm) is larger than for those deposited at 710 °C (≈300(50) nm). A large terrace size reduces the density of steeps. This reduction is important in SIS structures because they can act as pinholes or cuts in the barrier [10,19]. However, a small increment in the 3D topological defects reduces considerably the performance of the films for applications SIS devices using HTS.

Finally, it is important to discuss the superconducting transition temperature in our films (see Fig. 7). GBCO films with a thickness of 5 nm do not present superconducting transition. GBCO films with a thickness of 16 nm present a wide superconducting transition temperature of 83 (1) K (T_c, defined as 95% of the resistivity change) and an onset of 76 (1) K ($T_{c\text{-}on}$ defined as zero resistance). GBCO films with a thickness of 24 nm present an increment on the $T_c \approx 86.5$ (1) K, but the $T_{c\text{-}on}$ is slightly increased ≈77 (1) K. Finally the T_c is increased to 89.5 (1) K for thick films of 32 and 48 nm, whereas the $T_{c\text{-}on}$ is systematically reduced to 87 K. A 100 nm thick GBCO film shows a $T_c = 90.5$ K with a superconducting transition width ≈1.5 K. The thickness evolution of the T_c here reported can be explained by considering that stress at the interface with the substrate reduces the oxygen doping of the films [14,20]. The increment on the T_c for thicknesses above 20 nm is related with the growth of unstressed 3D structures and an increment in the oxygen content. The increment of 3D structures (as well the increment in their size) produces a gradual reduction in the superconductor transition width. Systematic changes in the superconducting transition width of films with and without STO buffer have not been observed, which indicates that the first unit cells of the films are stressed in both configurations [14]. It is important to note that higher T_c has been reported in very thin YBCO films by using other buffer layers [21–23]. In particular, a semiconductor $PrBa_2Cu_3O_{7-d}$ (PrBCO) buffer layer reduces the stress at the interface with the substrate and the T_c is enhanced due to Pr/Y interdiffusion (thick nominal superconductor layer) [21]. However, as PrBCO and YBCO on STO are isostructural chemical compounds, similar nucleation processes are expected among them.

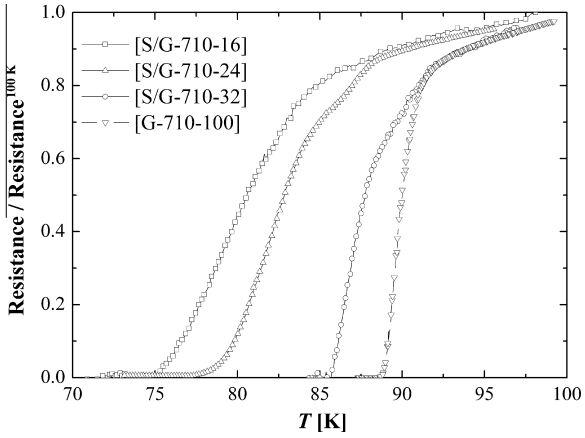

Fig. 7. Change of the normalized resistance/resistance (100 K) with temperature for the GBCO films with different thickness.

4. Conclusions

In summary, a detailed study of the structural, morphological and superconducting properties of very thin GBCO films has been performed. Two configurations were used: films with and without a STO ($t \approx 2$ nm) buffer layer. Detailed morphological studies indicate that the nucleation of 3D topological defects can be suppressed by the inclusion of a very thin STO buffer layer. This fact can be ascribed to the surface reconstruction of the substrate. The change in the surface termination of the STO modifies the first stages in the GBCO nucleation. The results obtained in buffered films are in agreement with a reduction of anti-phase boundaries (due to different interface stacking) between the GBCO and the STO. GBCO thin films with a thickness of 16 nm, presenting areas free of defects over $10 \times 10\ \mu m^2$ and a $T_{c\text{-}on} \approx 76$ (1) K were obtained. GBCO with thickness of ≈16 nm present the best combination of morphological (smooth surfaces) and superconducting properties (high T_c). These results contribute to improve the performance of HTS films in the design of SIS heterostructures.

Acknowledgments

This work was partially supported by the ANPCYT (PICT PRH 2008-109) and Universidad Nacional de Cuyo (06/C395). N.H. is member of the Instituto de Nanociencia y Nanotecnología (Argentina). M.S. and N.H. are members of CONICET (Argentina).

References

[1] M. Bibes, J.E. Villegas, A. Barthélèmy, Adv. Phys. 60 (2011) 5.
[2] J.P. Velev, S.S. Jawal, E.Y. Tsymbal, Philos. Trans. R. Soc. A 369 (2011) 3069.
[3] G. Xiao et al., Nature (London) 332 (1988) 238.
[4] X.H. Zhu, W. Peng, H.F. Tian, L.P. Yong, J. Li, J.Q. Li, D.N. Zheng, J. Phys. D: Appl. Phys. 39 (2006) 4222.
[5] Gang Xiao, M.Z. Cieplak, D. Musser, A. Gavrin, F.H. Streitz, C.L. Chien, J.J. Rhyne, J.A. Gotaas, Nature 332 (1988) 238.
[6] A.J. Kreisler, A.F. Dégardin, M. Aurino, C. Péroz, J.-C. Villégier, G. Beaudin, Y. Delorme, M. Redon, A. Sentz, Proc. IEEE Int. Microw. Symp. (2007) 345.
[7] M. Malnou, C. Feuillet-Palma, C. Ulysse, G. Faini, P. Febvre, M. Sirena, L. Olanier, J. Lesueur, N. Bergeal, J. Appl. Phys. 116 (2014) 074505.
[8] Guus Rijnders, Seve Currás, Mark Huijben, Dave H.A. Blank, Horst Rogalla, Appl. Phys. Lett. 84 (2004) 1150.
[9] M. Hawley, I.D. Raistrick, J.G. Beery, R.J. Houlton, Science 251 (1991) 1587.
[10] M. Sirena, L. Aviles Felix, N. Haberkorn, Appl. Phys. Lett. 103 (2013) 52902.
[11] J.A. Venables, G.D.T. Spiller, M. Hanbucken, Rep. Prog. Phys. 47 (1984) 399.
[12] X.-Y. Zheng, D.H. Lowndes, S. Zhu, J.D. Budai, R.J. Warmack, Phys. Rev. B 45 (1992) 7584.
[13] Miizeyyen Ece, Ester Garcia Gonzalez, Hanns-Ulrich Habermeier, Baybars Oral, J. Appl. Phys. 77 (1995) 1646–1649.
[14] V. Vonka, S.J. van Reeuwijk, J.M. Dekkers, S. Harkema, A.J.H.M. Rijnders, H. Graafsma, Thin Solid Films 449 (2004) 133–137.
[15] N. Haberkorn, G. Bridoux, E. Osquiguil, G. Nieva, J. Guimpel, Appl. Surf. Sci. 254 (2007) 222–224..
[16] Ryota Shimizu, Katsuyalwaya, Takeo Ohsawa, Susumu Shiraki, Tetsuya Hasegawa, TomihiroHashizume, Taro Hitosugi, ACS Nano 5 (2011) 7967.
[17] T. Ohsawa, K. Iwaya, R. Shimizu, T. Hashizume, T. Hitosugi, J. Appl. Phys. 108 (2010) 73710.
[18] O. Nakamura, Eric E Fullerton, J. Guimpel, Ivan K. Schuller, Appl. Phys. Lett. 60 (1992) 120.
[19] L. Avilés Félix et al., Nanotechnology 23 (2012) 495715.
[20] B. Wuyts, V.V. Moshchalkov, Y. Bruynseraede, Phys. Rev. B 53 (1996) 9418.
[21] I.N. Chan, D.C. Vier, O. Nakamura, J. Hasen, J. Guimpel, S. Schultz, Ivan K. Schuller, Phys. Lett. A 175 (1993) 241.
[22] I. Grekhov, M. Baydakova, V. Borevich, V. Davydov, L. Delimova, I. Liniichuk, A. Lyublinsky, Physica C 276 (1997) 18.
[23] C. Péroz, A.F. Dégardin, J.-C. Villégier, A.J. Kreisler, IEEE Trans. Appl. Supercond. 17 (2007) 637.